Temperature-dependent nanomechanics and topography of bacteriophage T7

Runing title: Temperature-dependent structure and mechanics of T7

Zsuzsanna Vörös, Gabriella Csík, Levente Herényi and Miklós Kellermayer

Department of Biophysics and Radiation Biology, Semmelweis University, Budapest H1094 Hungary

Corresponding author:

kellermayer.miklos@med.semmelweis-univ.hu

Abstract

Viruses are nanoscale infectious agents, which may be inactivated by heat treatment. The global molecular mechanisms of virus inactivation and the thermally-induced structural changes in viruses are not fully understood. Here we measured the heat-induced changes in the properties of T7 bacteriophage particles exposed to two-stage (65 ˚C and 80 ˚C) thermal effect, by using AFM-based nanomechanical and topographical measurements. We found that exposure to 65 ˚C led to the release of genomic DNA and to the loss of the capsid tail, hence the T7 particles became destabilized. Further heating to 80 ˚C surprisingly led to an increase in mechanical stability, due likely to partial denaturation of the capsomeric proteins kept within the global capsid arrangement.

Importance

Even though the loss of DNA, caused by heat treatment, destabilizes the T7 phage, its capsid is remarkably able to withstand high temperatures with a more-or-less intact global topographical structure. Thus, partial denaturation within the global structural constraints of the viral capsid may have a stabilizing effect. Understanding the structural design of viruses may help in constructing artificial nanocapsules for the packaging and delivery of materials under harsh environmental conditions.

Keywords

atomic force microscopy, nanoindentation, thermally-induced structural change, CD spectroscopy

Journal of Virology JVI Journal of Virology

Introduction

Viruses are remarkable nanoscale machineries that harbor a piece of genetic material within a proteinaceous capsule. As obligatory parasites, they are capable of efficiently fooling the host organism into manufacturing the viral structural elements, which spontaneously reproduce the virus particle by self-assembly. Because of their biological, medical and even economic importance, the properties of viruses have been investigated by a wide array of experimental approaches. It has long been known that most viruses can be thermally inactivated (1-4). It is hypothesized that thermal virus inactivation is caused by the release of the genetic material or some kind of capsid disruption (5-8), but the exact nature of the thermally-driven structural transitions within the viruses are little known. Differential scanning calorimetry and cryo-electron microscopy experiments have revealed a reversible structural transition at 53 ˚C limited to the hexamers of the HK97 bacteriophage (9). Heating the HK97 phage further results in the release of genomic DNA by not precisely known mechanisms, and heating even further to 80 ˚C results in an irreversible transition of thermal melting (10). In the case of bacteriophage λ, heat-induced transitions at 68 ˚C and 87 ˚C have been assigned to the escape of DNA and irreversible melting, respectively (11). The simultaneous observation of capsid- and DNA-related events, however, have not so far been possible at the level of the individual virus particles.

Previously, a distinct thermal melting of the bacteriophage T7 has been documented (12-15). T7 is a non-enveloped, short-tailed icosahedral *E.coli* phage that contains a 40 kbp genomic DNA (16). Thermal melting, measured by following OD_{260} as a function of temperature, involves two major transitions related to DNA. The first transition occurs between 50-60 ˚C, and it is thought to correspond to the release of DNA from the capsid. This transition is accompanied by a marked loss of infectivity (17). A second transition is detected in the

sample at temperatures above 80 ˚C, and it is related to DNA denaturation. Temperature-dependent CD spectroscopic measurements indicated that both of these transitions are likely to be accompanied by structural changes in the capsid proteins as well (12). Although high-resolution structural information is available on the protein capsid of T7 (18, 19), the details of the thermally-induced transitions within the protein components of the capsid remain unclear.

In recent years, atomic force microscopy (AFM)-based nanomechanical experiments emerged as a sensitive tool to explore the properties of viruses (20-29). It has been shown that nanomechanical parameters, such as stiffness and capsid breaking force, may reveal molecular mechanisms underlying capsid maturation, and the packaging, storage and release of genetic material.

Here we employed AFM to explore the nanomechanical and topographical changes in T7 bacteriophages exposed to two-stage thermal treatment (65 ˚C, 80 ˚C). We show that distinct changes in the nanomechanical properties of T7 occur upon heat treatment. Topographical analysis revealed the structural alterations that underlie the nanomechanical changes: 65 ˚C treatment leads to the release of genomic DNA and the loss of the tail complex, and further heating to 80 ˚C leads, on one hand, to the appearance of large globular particles that likely correspond to disassembled capsids and, on the other hand, to a partial structural stabilization of the remaining capsids, due most likely to rearrangements *via* partial denaturation of the capsomeric gp10A proteins.

Results and Discussion

Nanomechanics of heat-treated T7 phages

In the present work, individual, surface-adsorbed T7 phage particles exposed to different temperatures (room temperature, 65 ˚C, 80 ˚C) were manipulated with AFM to reveal their nanomechanical properties and the thermally-induced changes in these properties. **Fig. 1** shows our results obtained on phages at room temperature (RT). After landing the AFM tip on the capsid surface, force increased linearly to about 8 nN, where a sharp transition marked by a sudden drop of force and corresponding to capsid breakage occurred. Upon pressing the AFM tip further, force fluctuated below 2 nN, then it began to rise sharply upon approaching the substrate surface. The retraction force trace was essentially featureless; therefore, a large force hysteresis was present, indicating that the mechanical manipulation resulted in an irreversible conformational change (breakage) of the capsid. Although in the majority of the capsids similar force traces were recorded (**Fig. 1.c**), in a fraction of them we obtained traces with a significantly different, but reproducible, appearance (**Fig. 1.d**). In these traces the initial linear regime ended at about 2 nN (we refer to these as putative empty capsids, see below).

In T7 capsids treated at 65 ˚C (**Fig. 2.a-b**), the force traces were similar to those seen in **Fig. 1.d**: capsid breakage occurred at about 2 nN, then force fluctuated around 2 nN before increasing abruptly upon approaching the substrate surface. In T7 capsids heated further to 80 ˚C (**Fig. 2.c-d**), the overall appearance of the force traces was similar to that seen for the 65 ˚C samples, but capsid breakage and the following force fluctuation occurred at greater force levels.

Fig 3 displays the distribution of the parameters extracted from the force traces (see also **Table 1**). The breaking force values in the RT samples (**Fig. 3.a**) partition into two modes, according to the distinct types of force curves (see **Figs. 1.c-d**). The low-force mode of the

RT sample aligns well with the histogram peak of the 65 ˚C data (**Fig. 3.b**). Considering that T7 phages heated to temperatures above 60 ˚C are thought to loose their DNA (12), we tentatively conclude that the low-force peak in the RT data may correspond to empty capsids. The presence of empty capsids in the RT sample indicates that the spontaneous or artificially-induced DNA ejection of T7 phages is not negligible (30). The breaking force is severely reduced in 65 ˚C-treated capsids (from 6.90 nN to 1.61 nN, see **Table 1**). Since, according to AFM imaging results (see **Fig. 5**), the 65 ˚C treatment indeed resulted in the release of DNA from the capsids, our findings indicate that the presence of packaged DNA within the phage contributes to its mechanical stability. Quite interestingly, the breaking force was increased in the 80 ˚C-treated T7 phages relative to the ones treated at 65 ˚C (**Fig. 3.c**). Conceivably, structural rearrangements occurred in the capsomeric proteins between 65-80 ˚C, which resulted in a stabilization of their interactions, hence to an increased mechanical stability of the phage particle.

Stiffness was largest in the intact T7 phage, and the reduced stiffness values were similar in the RT empty capsids and the heat-treated ones (**Figs. 3.d-f**). Thus, the presence of packaged DNA contributes to the stiffness of the T7 phage.

The maximal indentation values progressively increased as a result of heat treatment (**Figs. 3.g-i**), which is a combined effect of the underlying changes in breaking forces and stiffness. Thus, even though the stiffness of 80 ˚C-treated T7 capsids is reduced, because of the increased breaking forces, they withstand greater indentations prior to breakage.

The mean capsid height became slightly reduced upon 65 ˚C treatment (**Fig. 3.j-k**). Notably, the mean capsid height of the empty-capsid RT phages is essentially identical to the 65 ˚C-treated ones, indicating that the presence of packaged DNA within the phage increases its diameter (by about 10 nm). Conceivably, the DNA pressure inside the phage causes the expansion of the icosahedral phage structure. We note that the 10 nm difference in mean

147 capsid height between the RT and 65 ˚C-treated capsids is only partly due to the DNA
148 pressure; since capsid height was obtained from mechanical measurements with a pyramidal
149 AFM tip, the presence of upward-oriented phage tails likely shifted the average height to
150 greater values in the RT samples. The capsid height is slightly increased in the 80 ˚C-treated
151 sample relative to 65 ˚C, which, as judged from the histogram shape (**Fig. 3.l**), is probably
152 due to the emergence of a subpopulation of capsids with larger diameter.
153
154 *AFM structure of heat-treated T7 phages*
155 To reveal the structural detail and mechanisms behind the heat-induced nanomechanical
156 changes in T7 capsids, we carried out high-resolution AFM measurements on phage particles
157 exposed to 65 ˚C and 80 ˚C (**Fig. 4.a**). In an overview AFM image of a typical RT sample
158 (**Fig. 4.b**), the characteristic T7 phage particles could be visualized against a nearly
159 featureless substrate background. Occasionally, a DNA molecule released from the capsid
160 upon mechanical perturbation could be observed. The mechanically-induced DNA ejection is
161 characterized by the sudden, within-one-scanline appearance of the DNA chain (30). We note
162 that there were a few globular particles in the background, which may correspond to the core
163 T7 phage proteins that become ejected simultaneously with DNA (30). Importantly, the
164 conical tail complex could be observed on most of the phage particles. Depending on the
165 surface binding of the phages, the tail complex was oriented in different directions (**Fig. 4.c**).
166 In high-resolution AFM images, even the size, the cogwheel shape and the central pore of the
167 capsomeres could be resolved (**Fig. 4.d-e**).
168 Upon 65 ˚C treatment, the topography of the background, and to some extent the capsids,
169 became different (**Fig. 5**). The most striking feature is that the substrate became covered with
170 a meshwork of DNA chains. A height profile of a section of the background (**Fig. 5.a inset**)
171 shows that the cross-sectional height of the individual strands is about 2 nm, which

demonstrates that they are indeed DNA. Thus, the 65 ˚C treatment, as suggested earlier (12), indeed resulted in the release of DNA from the T7 capsids. The second notable feature in the AFM images is that in most of the capsids the conical tail complex is not visible. Even if a tail can be seen, its structure is usually stubby, quite different from a cone (**Fig. 5.c**). Thus, DNA has been released from the phage particles, because of a separation of the tail complex from the capsid. Because the gp8 protein plays an important role in the connecting the tail complex to the capsid, we hypothesize that it might be a thermally sensitive component of T7. As a result, large (>10 nm) globular particles can be identified in the background, which may correspond to the remnants of the broken-off tail complexes. Although DNA release and the loss of tail were clearly observed in the samples treated at 65 ˚C, we do not exclude the possibility that these structural transitions may begin to occur at lower temperatures already (31, 32). We note that we were unable to detect the presence of L-shaped tail fibers on the substrate surface. Possibly, the poly-L-lysine-coated surface and the large amount of DNA precluded the binding of the tail fibers in proper orientation. The third striking feature is that the capsid surface became more faceted, and the icosahedron edges and faces emerged more distinctively (**Fig. 5.b**). Such a faceted appearance can be well explained by the shrinkage of the capsids upon DNA release (**Figs. 3.j-k**). In high-resolution AFM images, the cogwheel shape of the individual capsomeres could be well identified (**Figs. 5.d, f**). In a few capsids, we noticed gaps in the position of the pentameres, which are most likely the exit holes through which DNA escaped (**Fig. 5.e**).

In T7 samples exposed to 80 ˚C, the background was also densely populated with DNA strands (**Fig. 6.a**). A notable feature is the large number of globular particles scattered in the background. Even large aggregates of the particles could be observed (**Fig. 6.b**). Considering that the size of the aggregates far exceeds that of the tail complex, we hypothesize that the aggregates, hence their component globular particles, originate from the capsid wall. In high-

resolution AFM images (**Fig. 6.c-d**), the capsomeres appeared swollen, and they displayed less distinct cogwheel structure according to visual inspection. Altogether, the major transitions of T7 upon heating to 65 ˚C are the release of DNA rearrangements in the capsid. The transitions upon further heating to 80 ˚C entail structural changes within the capsid wall.

Analysis of topographical data

Representative height profiles across individual capsids (**Fig. 7.a**) demonstrate the heat-induced topographical changes in T7. Upon 65 ˚C treatment, the capsid slightly shrunk, its faces became flattened and its edges more distinct. The 80 ˚C-treated capsid shown here became swollen and its surface rugged. The ratio of capsids with visible tail complexes progressively reduced with heat treatment (**Fig. 7.b**). The capsomere diameter considerably increased after 80 ˚C treatment (**Fig. 7.c**). We hypothesize that thermally-induced conformational changes, most likely partial denaturation, has occurred in the gp10A capsomeric proteins, which resulted in an increase of their apparent volume. It might well be possible that the partial denaturation exposed the hydrophobic core of the capsomere proteins, and a hydrophobic interaction occurred in between neighboring capsomeres. Such an interaction may explain the increase in breaking force between 65 ˚C and 80 ˚C observed in the nanomechanical experiments (**Figs. 3.b-c**). The peak capsid height decreased slightly upon 65 ˚C treatment (**Figs. 7.d-e**), but the 80 ˚C treatment resulted in the emergence of a sub-population with larger height values (**Fig. 7.f**). We hypothesize that this sub-population corresponds to capsids with swollen wall structure. The peak capsid height analysis shown here more-or-less reflects the tendencies observed in the nanomechanical experiments. However, because AFM images allow us to select the tallest topographical point on the capsids, the peak height analysis is more sensitive to local variations, which are hidden or averaged out in the nanomechanics experiment.

222 The number of globular particles progressively increased in the samples upon heat treatment
223 (**Fig. 8.a**). The height of the major population of the particles is centered around 6 nm
224 regardless of heat treatment (**Figs. 8.b-d**). In the 80 ˚C-treated samples, particle populations
225 with much larger heights emerged (**Fig. 8.c**). While the ~6 nm particles may correspond to
226 the ejected core proteins, the large globular particles are most likely capsomeric proteins and
227 their aggregates, which appear due to the complete disassembly of some of the capsids.
228
229 *CD spectroscopic analysis*
230 To investigate the structural changes in heat-treated T7 further, CD spectroscopic
231 measurements were performed at room temperature (25 ˚C) and progressively increased
232 temperatures (61 ˚C, 83 ˚C) (**Fig 9**). The CD spectra, recorded at 25, 61 and 83 ˚C, display
233 differences in the short-wavelength regime (at 225 nm), indicating that capsid-protein-
234 associated structural transitions take place not only between 25-61 ˚C, but also between 61-83
235 ˚C. The latter appears to be part of a broad temperature-dependent transition that begins
236 slightly below 80 ˚C and peaks at 92 ˚C, and corresponds most likely to the loss of protein α-
237 helix content in a denaturing transition (12). In the AFM experiments, due to the brief (15
238 min) exposure to high temperature (80 ˚C) followed by cooling to room temperature, only
239 partial denaturation may have taken place.
240
241 *Model of thermally-induced structural changes in T7*
242 We propose the following phenomenological model to explain our observations (**Fig. 10**). At
243 room temperature (**Fig. 10.a**), T7 displays a characteristic icosahedral structure with
244 distinctive conical tail complex. The icosahedron is slightly swollen due to the DNA pressure
245 inside the capsid. The DNA-filled T7 phages have a high stiffness and withstand
246 (instantaneous) forces up to about 8 nN prior to breakage. Upon heating to 65 ˚C (**Fig. 10.b**),

the genomic DNA is ejected from the capsid. The release of DNA is likely caused by the conical tail complex breaking off the capsid, rather than by activating the natural DNA-ejection machinery. It is currently unclear whether the entire genome of T7 exits the capsid, or a portion remains inside. It is hypothesized that during its natural DNA ejection, only part of the T7 genome is driven out of the capsid due to the DNA pressure. The remaining DNA is thought to be pulled into the *E.coli* by an active process (33-35). However, because the thermally-induced changes involve the loss of the entire tail complex, there might be enough room for the nearly complete release of the T7 genome. Regardless of how much DNA exits during this process, the resulting drop in DNA pressure is accompanied by a shrinkage and a more faceted appearance of the capsid. Upon further heating to 80˚C (**Fig. 10.c**) the capsids do not disappear, but they are still present with a maintained global structure. A partial denaturation likely takes place in the gp10A proteins that form the capsomeres and hence the capsid wall. The partial protein denaturation within the global confinement of the capsid architecture, and the resulting exposure of hydrophobic protein regions result in capsomere swelling and a new set of inter-capsomeric interactions, most probably *via* hydrophobic protein regions. Facilitated folding and misfolding following repetitive partial or complete denaturation have been observed in proteins confined either in a chaperonin system (36) or in a force field (37). Notably, capturing a protein in the misfolded state results in a considerable conformational expansion (38). We envision that similar processes may occur in the gp10A proteins heated to 80˚C, then cooled to room temperature. In the end, the capsid wall becomes thicker, and the entire capsid surface becomes rugged. It is quite conceivable, that the hydrophobic stabilization is not the result of the heating *per se*, but of the relaxation from the thermal exposure. That is, capsids that did not completely fall apart during the 80 ˚C treatment may relax into a stabilized structure upon cooling back to

room temperature. By adjusting the time of exposure to the high temperature, the capsid stabilization may conceivably be tuned.

Conclusions

We have directly shown that exposing T7 to a thermal treatment at 65 ˚C caused the release of its genomic DNA due to the tail complex breaking off the capsid. The loss of DNA and/or thermally-driven changes in capsomeric protein structure result in a reduced capsid stiffness and breaking force. Further heating to 80 ˚C leads to rearrangements within the capsid wall, caused most likely by partial denaturation of the component gp10A proteins. Even though the the capsids are destabilized, they are remarkably able to still withstand high temperatures with a more-or-less intact global topographical structure. Thus, partial denaturation within the global structural constraints of the viral capsid may have a stabilizing effect. Understanding the structural design of viruses may help in constructing artificial nanocapsules for the packaging and delivery of materials under harsh environmental conditions. By tuning capsid stability, these nanocapsules may, in principle, be tailored for specific applications.

287 **Materials and methods**

288 *T7 preparation*

289 T7 (ATCC 11303-B7) was grown in *Escherichia coli* (ATCC 11303) host cells and purified
290 according established methods (39). Briefly, the phage suspension was concentrated on a
291 CsCl gradient and dialyzed against buffer (20 mM Tris-HCl, 50 mM NaCl, pH 7.4) (14) . T7
292 bacteriophage concentration was determined from optical density by using an exctinction
293 coefficient of $\varepsilon_{260} = 7.3 \times 10^3$ (mol nucleotide bases $\times$ $L^{-1} \times cm^{-1}$). The dialyzed T7 samples
294 were kept at 4 ˚C for a few months without significant loss of activity. Prior to further use the
295 T7 samples were diluted with PBS (137 mM NaCl, 2.7 mM KCl, 10 mM Na_2HPO_4, 1.8 mM
296 KH_2PO_4, pH 7.4).

297

298 *Atomic force microscopy and nanomanipulation*

299 T7 samples properly diluted in PBS were applied to freshly cleaved mica functionalized with
300 glutaraldehyde (29, 40). The dilution was adjusted so that an approximate surface density of
301 10 phage particles per μm^2 is achieved. A freshly-cleaved mica was first incubated with poly-
302 L-lysine (0.01 % aqueous solution) for 20 minutes at room temperature, then rinsed
303 extensively with MilliQ water and dried with a stream of high-purity N_2 gas. Subsequently,
304 the surface was incubated with 10 % aqueous glutaraldehyde for 30 minutes at room
305 temperature, then rinsed extensively with MilliQ water and dried with a stream of high-purity
306 N_2 gas. Finally, a sample of T7 phage was loaded onto the substrate surface and incubated for
307 40 minutes on ice. Unbound viruses were removed by gentle washing with PBS. Non-contact
308 mode AFM images were acquired with an Asylum Research Cypher instrument (Asylum
309 Research, Santa Barbara, CA) by using silicon-nitride cantilevers (Olympus BL-AC40TS-C2
310 or Nanoworld PNP-TR). 512 x 512-pixel images were collected at a typical scanning
311 frequency of 0.3-1.5 Hz and with a mean indentation force of about 30 pN. All of the images

312 presented in this work were collected on non-fixed samples under aqueous buffer conditions.
313 For temperature-dependent measurements we used the cooler/heater stage of the AFM
314 instrument. Temperature was kept constant with a precision of 0.1 ˚C. Evaporation of water
315 was prevented by the sealed container housing the AFM scanner. For nanomechanical
316 measurements the surface-bound viruses were manipulated by first pressing the cantilever
317 (Nanoworld PNP-TR, lever 1) tip against the apex of the virus, then pulling the cantilever
318 away with a constant, pre-adjusted rate (29). Typical cantilever movement rate was 1 μm/s
319 except where noted otherwise. Stiffness was determined for each cantilever by using thermal
320 method (41).
321
322 *Image processing and data analysis*
323 AFM images and force spectra were analyzed using algorithms built in the Cypher controller
324 software (AsylumResearch, Santa Barbara, CA). Indentation distance (z) was calculated from
325 cantilever displacement (s), force (F) and cantilever stiffness (k) as
326 $$z=s-F/\kappa. \quad (1)$$
327 AFM images were corrected for flatness of field (within a few Å) and their color contrast was
328 adjusted in order to better communicate the relevant features. No additional image processing
329 was carried out.
330
331 *CD spectroscopy*
332 Circular dichroism measurements were carried out on a Jasco J-810 dichrograph in 1 cm
333 quartz cell. The solvent reference spectra were automatically subtracted from the CD spectra
334 of the samples. The solvent was a buffer containing 20 mM TRIS and 50 mM NaCl (pH 7.4).
335 Temperature was controlled with a PFD-425S type Peltier heating system. For temperature-
336 controlled measurements, the sample cell was equilibrated for 3 minutes at the target

temperature prior to data acquisition. CD band intensities were expressed in molar ellipticity, Θ (deg·cm^{2}·dmol^{-1}). Spectra were smoothed by the Savitzky-Golay algorithm.

Statistics

The number of nanomechanical curves, images and particles (T7 or globular) analyzed are shown in the relevant figures. The results shown in this manuscript were collected in 15 independent nanomechanics and 9 independent AFM imaging experiments. The CD spectra are the average of three scans. CD data were analyzed by using the Microcal Origin software (OriginLab, Northampton, MA). Statistical analyses and graph plotting was carried out by using either KaleidaGraph (v.4.5.1, Synergy Software, Reading, PA) or IgorPro (v. 6.34A, Wavementrics, Lake Oswego, OR) programs.

Acknowledgements

This work was supported by grants from the Hungarian National Research, Development and Innovation Office (K109480; K124966; VKSZ_14-1-2015-0052; NVKP-16-1-2016-0017 National Heart Program). The research leading to these results has received funding from the European Union's Seventh Framework Program (FP7/2007-2013) under grant agreement n° HEALTH-F2-2011-278850 (INMiND).

Z.V. performed research, analyzed data, and wrote the paper; G.C. performed research, contributed analytic tools, and wrote the paper; L.H. analyzed data and wrote the paper; M.K. designed research, performed research, analyzed data, and wrote the paper.

References

1. **Foster RAC**, **Johnson FH**, **Miller VK**. 1949. The influence of hydrostatic pressure and urethane on the thermal inactivation of bacteriophage. J Gen Physiol **33**:1–16.

2. **Pollard EC**, **Solosko W**. 1971. The thermal inactivation of T4 and lambda bacteriophage. Biophysj **11**:66–74.

3. **Yamagishi H**, **Ozeki H**. 1972. Comparative study of thermal inactivation of phage phi 80 and lambda. Virology **48**:316–322.

4. **Wetzel R**, **Perry LJ**, **Baase WA**, **Becktel WJ**. 1988. Disulfide bonds and thermal stability in T4 lysozyme. Proc Natl Acad Sci USA **85**:401–405.

5. **Brié A**, **Bertrand I**, **Meo M**, **Boudaud N**, **Gantzer C**. 2016. The Effect of Heat on the Physicochemical Properties of Bacteriophage MS2. Food Environ Virol **8**:251–261.

6. **Wigginton KR**, **Kohn T**. 2012. Virus disinfection mechanisms: the role of virus composition, structure, and function. Curr Opin Virol **2**:84–89.

7. **Pfaender S**, **Brinkmann J**, **Todt D**, **Riebesehl N**, **Steinmann J**, **Steinmann J**, **Pietschmann T**, **Steinmann E**. 2015. Mechanisms of methods for hepatitis C virus inactivation. Appl Environ Microbiol **81**:1616–1621.

8. **Wigginton KR**, **Pecson BM**, **Sigstam T**, **Bosshard F**, **Kohn T**. 2012. Virus inactivation mechanisms: impact of disinfectants on virus function and structural integrity. Environ Sci Technol **46**:12069–12078.

9. **Conway JF**, **Cheng N**, **Ross PD**, **Hendrix RW**, **Duda RL**, **Steven AC**. 2007. A thermally induced phase transition in a viral capsid transforms the hexamers, leaving the pentamers unchanged. J Struct Biol **158**:224–232.

10. **Duda RL**, **Ross PD**, **Cheng N**, **Firek BA**, **Hendrix RW**, **Conway JF**, **Steven AC**. 2009. Structure and Energetics of Encapsidated DNA in Bacteriophage HK97 Studied by Scanning Calorimetry and Cryo-electron Microscopy. J Mol Biol **391**:471–483.

11. **Qiu X**. 2012. Heat induced capsid disassembly and DNA release of bacteriophage λ. PLoS ONE **7**:e39793.

12. **Csík G**, **Egyeki M**, **Herényi L**, **Majer Z**, **Tóth K**. 2009. Role of structure-proteins in the porphyrin-DNA interaction. J Photochem Photobiol B, Biol **96**:207–215.

13. **Tóth K**, **Rontó G**. 1987. Salt effects on bacteriophage T7-I. Physiol Chem Phys Med NMR **19**:59–66.

14. **Tóth K**, **Csik G**, **Rontó GY**. 1987. Salt effects on the bacteriophage T7-II structure and activity changes. Physiol Chem Phys Med NMR **19**:67–74.

15. **Zupán K**, **Herényi L**, **Tóth K**, **Majer Z**, **Csík G**. 2004. Binding of cationic porphyrin to isolated and encapsidated viral DNA analyzed by comprehensive spectroscopic methods. Biochemistry **43**:9151–9159.

16. **Cerritelli ME**, **Cheng N**, **Rosenberg AH**, **McPherson CE**, **Booy FP**, **Steven AC**. 1997. Encapsidated conformation of bacteriophage T7 DNA. Cell **91**:271–280.

17. **Fekete A**, **Rontó G**, **Feigin LA**, **Tikhonychev VV**, **Módos K**. 1982. Temperature dependent structural changes of intraphage T7 DNA. Biophys Struct Mech **9**:1–9.

18. **Agirrezabala X**, **Velázquez-Muriel JA**, **Gómez-Puertas P**, **Scheres SHW**, **Carazo JM**, **Carrascosa JL**. 2007. Quasi-Atomic Model of Bacteriophage T7 Procapsid Shell: Insights into the Structure and Evolution of a Basic Fold. Structure **15**:461–472.

19. **Guo F**, **Liu Z**, **Fang PA**, **Zhang Q**, **Wright ET**, **Wu W**, **Zhang C**, **Vago F**, **Ren Y**, **Jakana J**, **Chiu W**, **Serwer P**, **Jiang W**. 2014. Capsid expansion mechanism of bacteriophage T7 revealed by multistate atomic models derived from cryo-EM reconstructions. Proc Natl Acad Sci U S A **111**:E4606–E4614.

20. **Michel JP**, **Ivanovska IL**, **Gibbons MM**, **Klug WS**, **Knobler CM**, **Wuite GJL**, **Schmidt CF**. 2006. Nanoindentation studies of full and empty viral capsids and the effects of capsid protein mutations on elasticity and strength. Proc Natl Acad Sci USA **103**:6184–6189.

21. **Kol N**, **Gladnikoff M**, **Barlam D**, **Shneck RZ**, **Rein A**, **Rousso I**. 2006. Mechanical properties of murine leukemia virus particles: effect of maturation. Biophysj **91**:767–774.

22. **Ivanovska IL**, **Miranda R**, **Carrascosa JL**, **Wuite GJL**, **Schmidt CF**. 2011. Discrete fracture patterns of virus shells reveal mechanical building blocks. Proc Natl Acad Sci U S A **108**:12611–12616.

23. **Kurland NE**, **Drira Z**, **Yadavalli VK**. 2012. Measurement of nanomechanical properties of biomolecules using atomic force microscopy. Micron **43**:116–128.

24. **Castellanos M**, **Pérez R**, **Carrasco C**, **Hernando-Perez M**, **Gómez-Herrero J**, **de Pablo PJ**, **Mateu MG**. 2012. Mechanical elasticity as a physical signature of conformational dynamics in a virus particle. Proc Natl Acad Sci U S A **109**:12028–12033.

25. **Mateu MG**. 2012. Mechanical properties of viruses analyzed by atomic force microscopy: a virological perspective. Virus Res **168**:1–22.

26. **Cieplak M**, **Robbins MO**. 2013. Nanoindentation of 35 virus capsids in a molecular model: relating mechanical properties to structure. PLoS ONE **8**:e63640.

27. **Hernando-Pérez M**, **Lambert S**, **Nakatani-Webster E**, **Catalano CE**, **de Pablo PJ**. 2014. Cementing proteins provide extra mechanical stabilization to viral cages. Nat Commun **5**.

28. **Ramalho R**, **Rankovic S**, **Zhou J**, **Aiken C**, **Rousso I**. 2016. Analysis of the mechanical properties of wild type and hyperstable mutants of the HIV-1 capsid. Retrovirology 1–7.

29. **Vörös Z**, **Csík G**, **Herényi L**, **Kellermayer MSZ**. 2017. Stepwise reversible nanomechanical buckling in a viral capsid. Nanoscale **9**:1136–1143.

30. **Kellermayer MSZ**, **Vörös Z**, **Csík G**, **Herényi L**. 2018. Forced phage uncorking: viral DNA ejection triggered by a mechanically sensitive switch. Nanoscale **10**:1898–1904.

31. **Serwer P**. 1976. Internal proteins of bacteriophage T7. J Mol Biol **107**:271–291.

32. **Steven AC**, **Trus BL**, **Maizel JV**, **Unser M**, **Parry DA**, **Wall JS**, **Hainfeld JF**, **Studier FW**. 1988. Molecular substructure of a viral receptor-recognition protein. The gp17 tail-fiber of bacteriophage T7. J Mol Biol **200**:351–365.

33. **Molineux IJ**. 2001. No syringes please, ejection of phage T7 DNA from the virion is enzyme driven. Molecular Microbiology **40**:1–8.

34. **Molineux IJ**, **Panja D**. 2013. Popping the cork: mechanisms of phage genome ejection. Nat Rev Microbiol **11**:194–204.

35. **Molineux IJ**. 2006. Fifty-three years since Hershey and Chase; much ado about pressure but which pressure is it? Virology **344**:221–229.

36. **Lin Z**, **Puchalla J**, **Shoup D**, **Rye HS**. 2013. Repetitive protein unfolding by the trans ring of the GroEL-GroES chaperonin complex stimulates folding. Journal of Biological Chemistry **288**:30944–30955.

37. **Oberhauser AF**, **Marszalek PE**, **Carrion-Vazquez M**, **Fernandez JM**. 1999. Single protein misfolding events captured by atomic force microscopy. Nat Struct Biol **6**:1025–1028.

38. **Hammarstrom P**, **Persson M**, **Carlsson U**. 2001. Protein compactness measured by fluorescence resonance energy transfer. Human carbonic anhydrase ii is considerably expanded by the interaction of GroEL. J Biol Chem **276**:21765–21775.

39. **Strauss JH**, **Sinsheimer RL**. 1963. Purification and properties of bacteriophage MS2 and of its ribonucleic acid. J Mol Biol **7**:43–54.

40. **Wang H**, **Bash R**, **Yodh JG**, **Hager GL**, **Lohr D**, **Lindsay SM**. 2002. Glutaraldehyde modified mica: a new surface for atomic force microscopy of chromatin. Biophysj **83**:3619–3625.

41. **Matei GA**, **Thoreson EJ**, **Pratt JR**, **Newell DB**, **Burnham NA**. 2006. Precision and accuracy of thermal calibration of atomic force microscopy cantilevers. Review of Scientific Instruments **77**:083703.

469 42. **Vörös Z, Csík G, Herényia L, Kellermayer MSZ.** 2017. Stepwise reversible
470 nanomechanical buckling in a viral capsid. Nanoscale **9**:1136–1143.

471

472 **Figure legends**

473

474 **Figure 1.** Nanomechanics of T7 phages. **a.** Schematics of mechanical manipulation: the tip of
475 the AFM cantilever is first brought into contact with the T7 phage surface (i) which is then
476 pressed (ii) with a pre-adjusted velocity to 10 nN maximal force during which the capsid
477 eventually ruptures (iii). Finally the cantilever is lifted (iv). AFM cantilever and T7 phage are
478 not to scale. **b.** Representative force *versus* indentation curve obtained at room temperature.
479 Data collected during the indentation half-cycle is displayed in red, whereas those during
480 retraction in blue. Notable stages of the nanomechanics experiments are shown with small
481 Roman numerals (i-iv). Variables extracted from the data (breaking force *F*, maximal
482 indentation distance *x*, capsid height *h*) are shown with italic letters. Capsid stiffness (*k*) is
483 obtained by fitting a line in the initial linear regime of the indentation data (ii). **c.** Dataset
484 containing 80 similar, overlaid force *versus* indentation curves collected in independent
485 experiments on different phage particles at room temperature (42). Red and blue traces are
486 indentation and retraction half cycles, respectively. **d.** Dataset containing 55 similar, overlaid
487 force *versus* indentation curves (indentation half cycle only), collected at room temperature in
488 independent experiments, which are similar to each other but are distinctively different from
489 the dataset in c (putatively called empty-capsid curves, see later).

490

491 **Figure 2.** Nanomechanics data of heat-treated T7 phages. Red and blue indicate indentation
492 and retraction half-cycles, respectively. **a.** Representative force *versus* indentation curve
493 measured on a T7 phage particle that has been exposed to a temperature of 65 ˚C for 15
494 minutes. **b.** Dataset containing 45 similar, overlaid force *versus* indentation curves collected
495 in independent experiments on different phage particles heat-treated at 65 ˚C. **c.**
496 Representative force *versus* indentation curve measured on a T7 phage particle that has been

497 exposed to a temperature of 80 ˚C for 15 minutes. **d.** Dataset containing 41 similar, overlaid
498 force *versus* indentation curves collected in independent experiments on different phage
499 particles heat-treated at 80 ˚C.
500
501 **Figure 3.** Distribution of variables obtained from nanomechanics data. Breaking force (**a, b,**
502 **c**), stiffness (**d, e, f**), maximal indentation distance (**g, h, i**) and capsid height (**j, k, l**)
503 histograms for T7 phage particles at room temperature (RT) and ones treated at 65 ˚C and 80
504 ˚C, respectively. Light gray bars correspond to data obtained on empty capsids at room
505 temperature. The numbers (n) refer to the number of force curves analyzed to obtain the
506 nanomechanical parameters.
507
508 **Figure 4.** Temperature-dependent AFM measurements on T7 phage particles. **a**. Thermal
509 treatment protocol. Sample temperature *versus* time trace recorded in a typical experiment.
510 The same sample is exposed to consecutive heating (for 15 min) cooling (to 20 ˚C) and image
511 acquisition (at 20 ˚C) cycles. **b.** Overview of a 1 µm x 1 µm sample area at room temperature
512 (20 ˚C). Slow AFM raster scan direction is from top to bottom of the image. White arrowhead
513 points at the nearly instantaneous event of mechanically induced DNA ejection. Scale bar 100
514 nm. **Inset**, topographical height map along an arbitrarily chosen line in the background (white
515 dashed line). **c.** AFM images of T7 phage particles displaying their conical tail in different
516 orientations. White arrowheads point at the tail apices. Scale bar 30 nm. **d.** High-resolution
517 AFM images of the T7 phage surfaces with resolvable capsomeres. Views along the two-fold
518 (i, ii) and three-fold symmetry axes (iii), which are explained in (iv), are shown. Scale bar 10
519 nm. In the bottom row dashed guiding lines are superimposed on the respective images to
520 indicate the symmetries. **e.** Magnified view of a cogwheel-shaped hexagonal capsomere.
521 Arrowheads point at the spokes of the cogwheel. Scale bar 10 nm.

Figure 5. AFM of T7 phages treated at 65 ˚C. **a.** Overview of a 1 µm x 1 µm sample area. White arrowheads point at large (>10 nm) globular particles. Scale bar 100 nm. **Inset**, topographical height map along an arbitrarily chosen line in the background (white dashed line). Black arrowheads point at DNA cross-sections, whereas the empty arrowhead at the substrate (mica) surface. **b.** Comparison of icosahedral facets of room-temperature (i) and 65-degree (ii) capsids. AFM images contrast enhanced with identical color-scale offset (48 nm) and range (20 nm). **c.** AFM image of two T7 particles. White arrowhead points at the short, stubby tail complex visible on one of the particles whereas there is no visible tail on the other one. Scale bar 20 nm. **d.** High-resolution AFM images of 65 ˚C-treated T7 phage particles with resolvable capsomeres on their surfaces. Views are along the three-fold symmetry axes. Because of contrast enhancement, only the top facets are visible and the rest of the capsid is hidden. Scale bar 10 nm. **e.** T7 particles with resolvable DNA exit holes (white arrowheads). The exit hole appears as a gap in the location of a missing pentagonal capsomere at one of the icosahedron vertices. Images viewed along the two-fold (i), three-fold (ii, iii, iv) and five-fold symmetry axes (v, vi) are shown. Images iii and v are reconstructed from the rightward fast AFM scanlines, whereas images iv and vi are from leftward (reverse) scanlines from the same sample area. Scale bars, 20 nm. **f.** Magnified view of a cogwheel-shaped hexagonal capsomere. Arrowheads point at the spokes of the cogwheel. Scale bar 10 nm.

Figure 6. AFM of T7 phages treated at 80 ˚C. **a.** Overview of a 1 µm x 1 µm sample area. White arrowheads point at large (>10 nm) globular particles. Scale bar 100 nm. **b.** AFM image showing large aggregates of globular particles (white arrowheads) **c.** High-resolution AFM images of 80-degree-treated T7 phage particles with resolvable capsomeres on their surface. Views along the three-fold (i, iii) and two-fold symmetry axes (ii) are shown. Scale

bar 10 nm. **d.** Magnified view of the capsomeric structure. Arroheads point at putative spokes of the originally cogwheel-shaped capsomere. Note that the central pore cannot be resolved, most likely due to the swelling of the protein matrix. Scale bar 10 nm.

Figure 7. Analysis of capsid topography data. **a.** Topographical height map along the cross-section of either a capsid at room temperature (green trace) or ones treated at 65 ˚C (orange) or 80 ˚C (red). **b.** Ratio of capsids with tails as a function of temperature. The numbers above the bars represent the number of fields analyzed for every T7 particle. Error bars represent standard deviation (SD). **c.** Capsomer diameter as a function of temperature. The numbers above the bars represent the number of capsomers measured. Error bars represent standard deviation (SD). **d, e** and **f** show histograms of peak capsid heights for room-temperature (RT), 65 ˚C and 80 ˚C treated T7 phages, respectively. Peak height refers to the tallest topographical point in the capsid image. The numbers (n) refer to the number of T7 phage particles analyzed.

Figure 8. Analysis of topographical data of globular particles. **a.** Number of globular particles per field as a function of temperature. The numbers above the bars represent the number of fields analyzed for every particle. Error bars represent standard deviation (SD). **b, c** and **d** show histograms of globular particle height for samples at room temperature (RT) and ones treated at 65 ˚C and 80 ˚C, respectively. Black arrowheads point at populations of large globular particles. The numbers (n) refer to the number of globular particles analyzed.

Figure 9. CD spectroscopy of heat-treated T7. CD spectra of T7 samples recorded at room temperature (25 ˚C, black line), at 61 ˚C (blue line) and 83 ˚C (red line). Arrow marks the wavelength of 225 nm, at which the protein-dependent changes were monitored.

Journal of Virology JVI Journal of Virology

572

573 **Figure 10.** Schematic model of thermally-induced changes in the T7 bacteriophage. At room
574 temperature (**a**) the capsid is slightly swollen because of the DNA pressure inside. The
575 bulging of the capsid wall as shown in the scheme is not to scale. Upon heating to and
576 incubating at a temperature of 65 ˚C (**b**), the tail complex is broken off, resulting in the
577 release of the genomic DNA. The capsid becomes more faceted due to the relaxation of the
578 capsid pressure. Finally, at 80 ˚C (**c**) the capsid becomes swollen and its surface irregular, and
579 the capsids may become fragmented into large globular particles (this last step is not shown).

580

581 **Table 1.** Nanomechanical and topographical parameters of T7 bacteriophage capsids and
582 globular particles (mean ±S.D.).
583

	RT (DNA-filled)	RT (empty)	65 ˚C	80 ˚C
Nanomechanics				
Breaking force (*F*, nN)	6.90 ± 0.97	1.90 ± 0.34	1.61 ± 0.52	3.83 ± 1.20
Capsid stiffness (*k*, Nm^{-1})	0.73 ± 0.12	0.36 ± 0.10	0.27 ± 0.11	0.35 ± 0.15
Maximal indentation (*x*, nm)	13.24 ± 2.13	9.51 ± 2.41	12.56 ± 4.70	22.97 ± 6.61
Capsid height (*h*, nm)	60.4 ± 1.71	59.93 ± 1.56	59.41 ± 4.00	60.71 ± 4.87
Capsid topography				
Ratio of tailed capsids	0.83 ± 0.1	NA	0.19 ± 0.12	0.05 ± 0.06
Peak capsid height (nm)	61.8 ± 3.6	NA	58.2 ± 1.7	63.3 ± 5.5
Capsomer diameter (nm)	11.0 ± 0.8	NA	9.8 ± 1.0	13.9 ± 2.2
Globular particle parameters				
Particle height (nm)	7.6 ± 3.2	NA	6.9 ± 2.5	10.0 ± 5.4

584

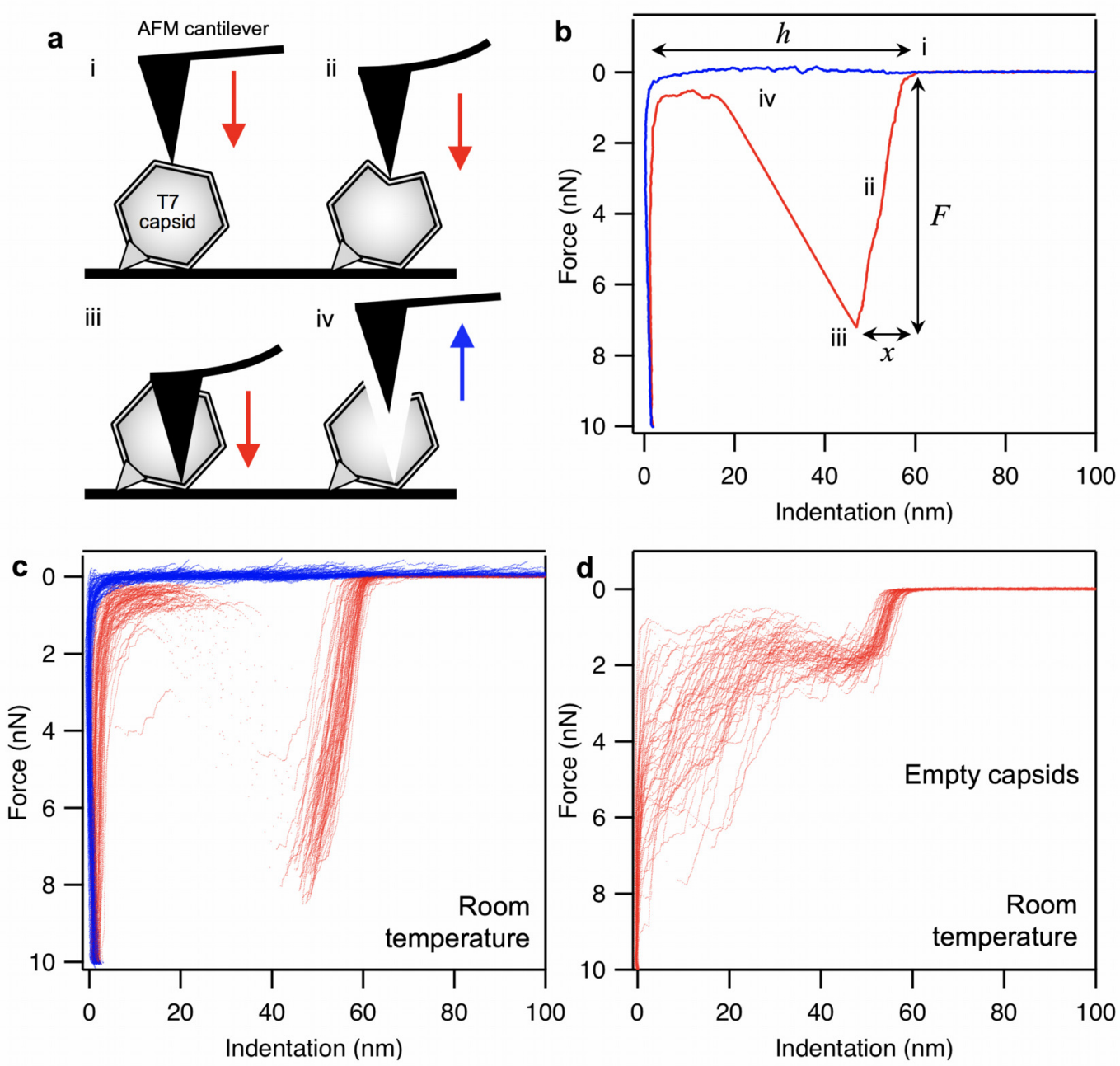

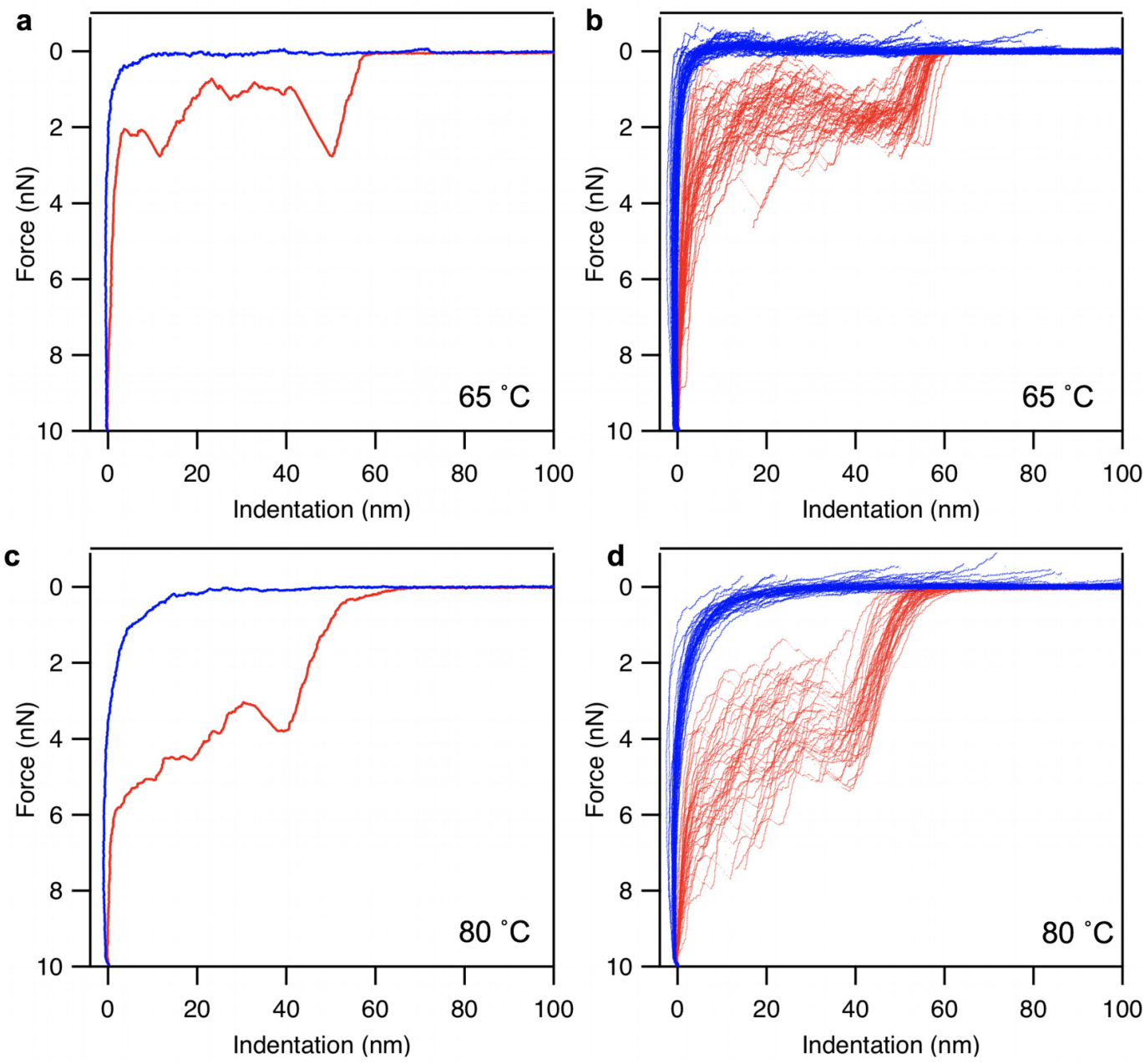

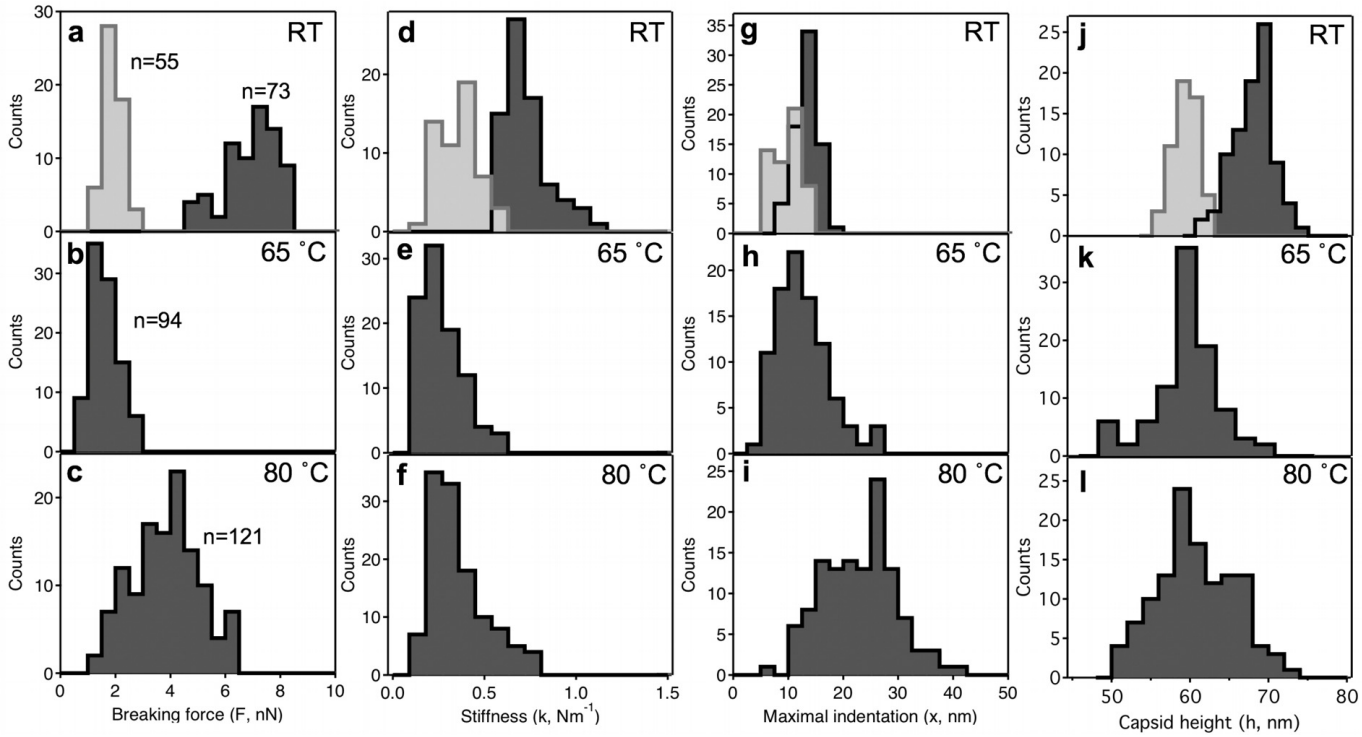

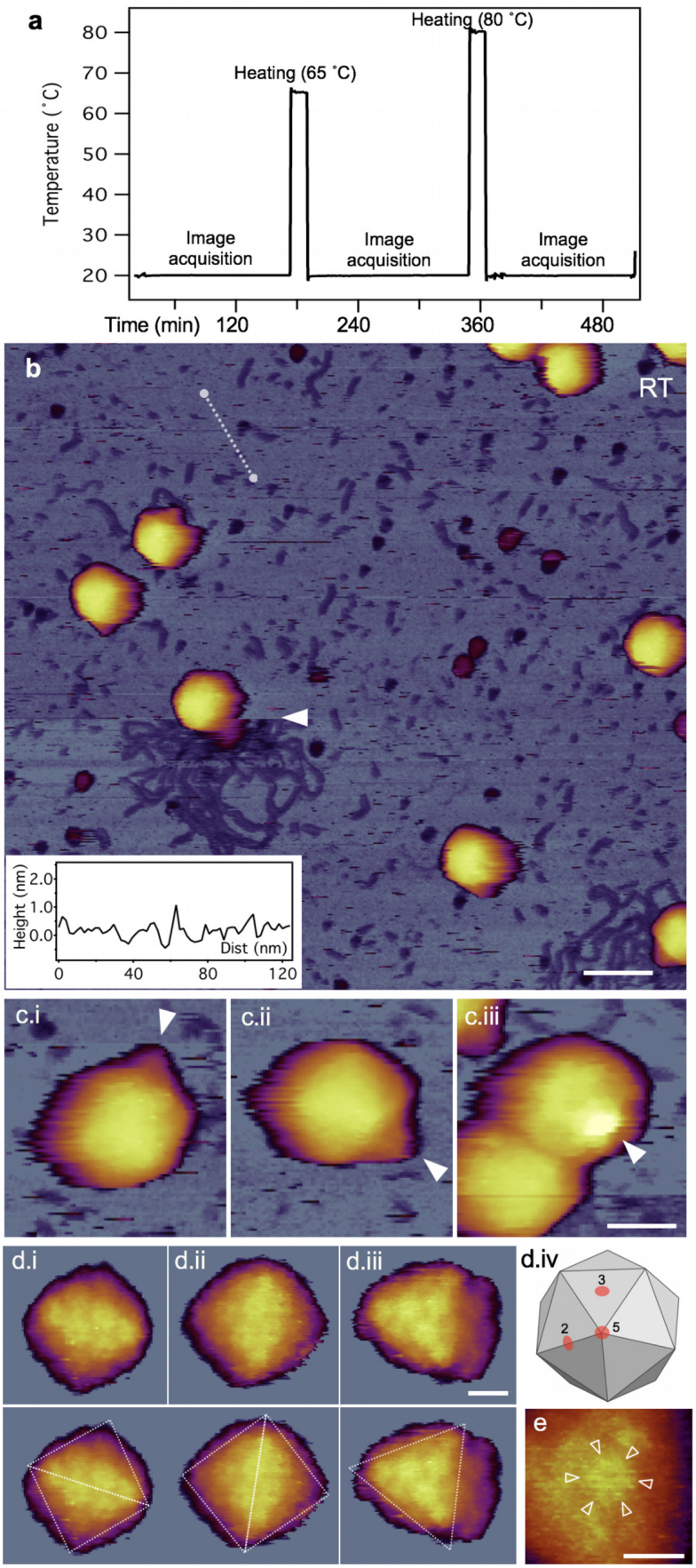

Journal of Virology

JVI

Journal of Virology

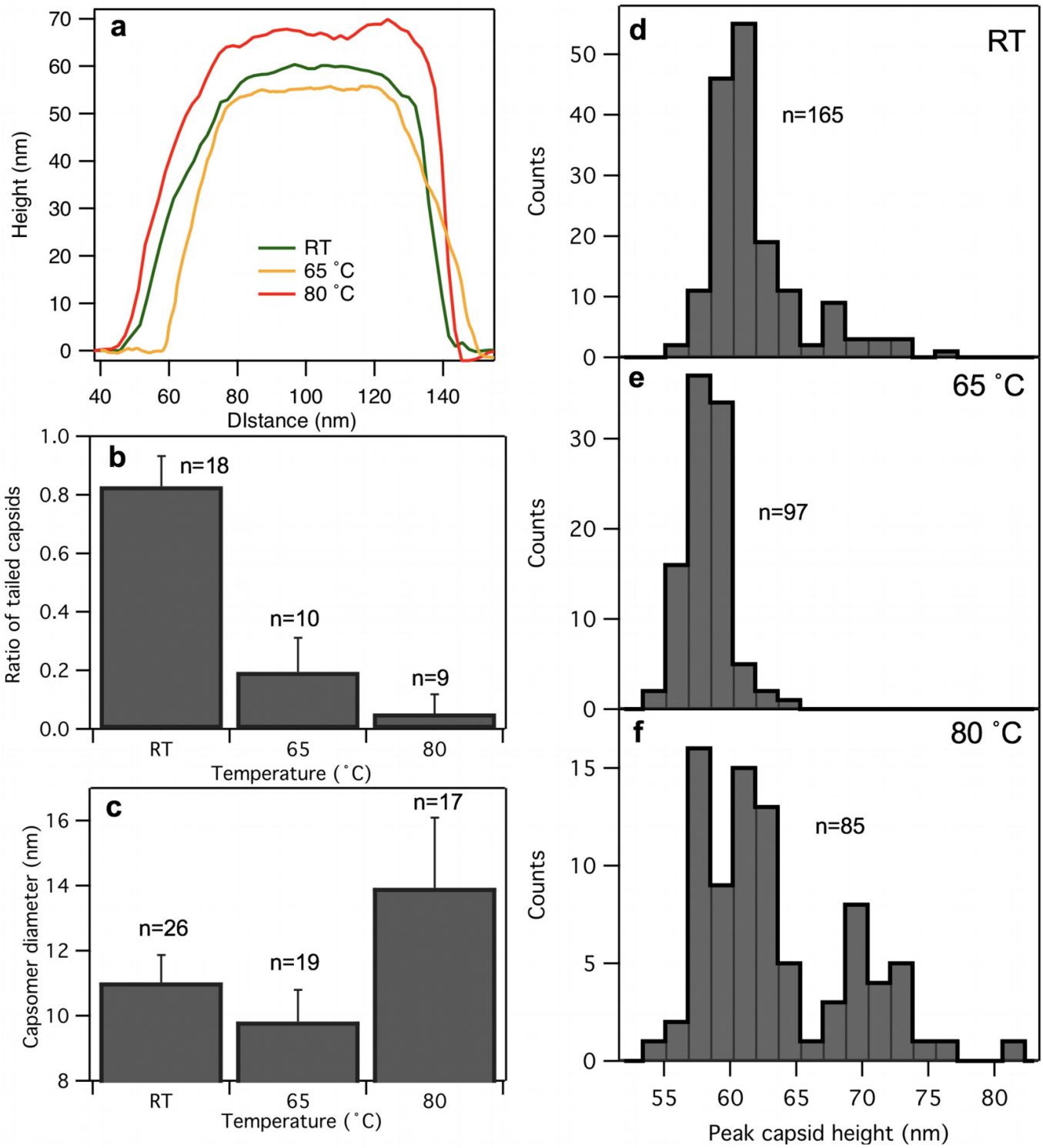

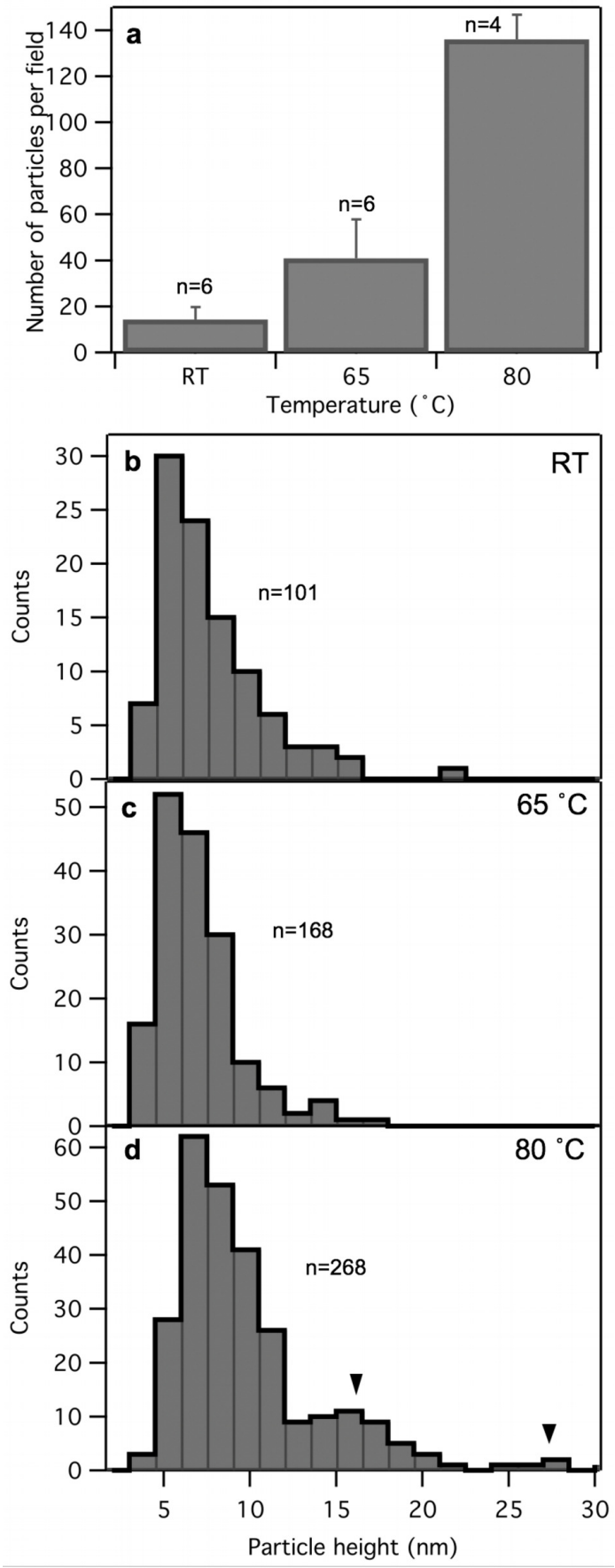

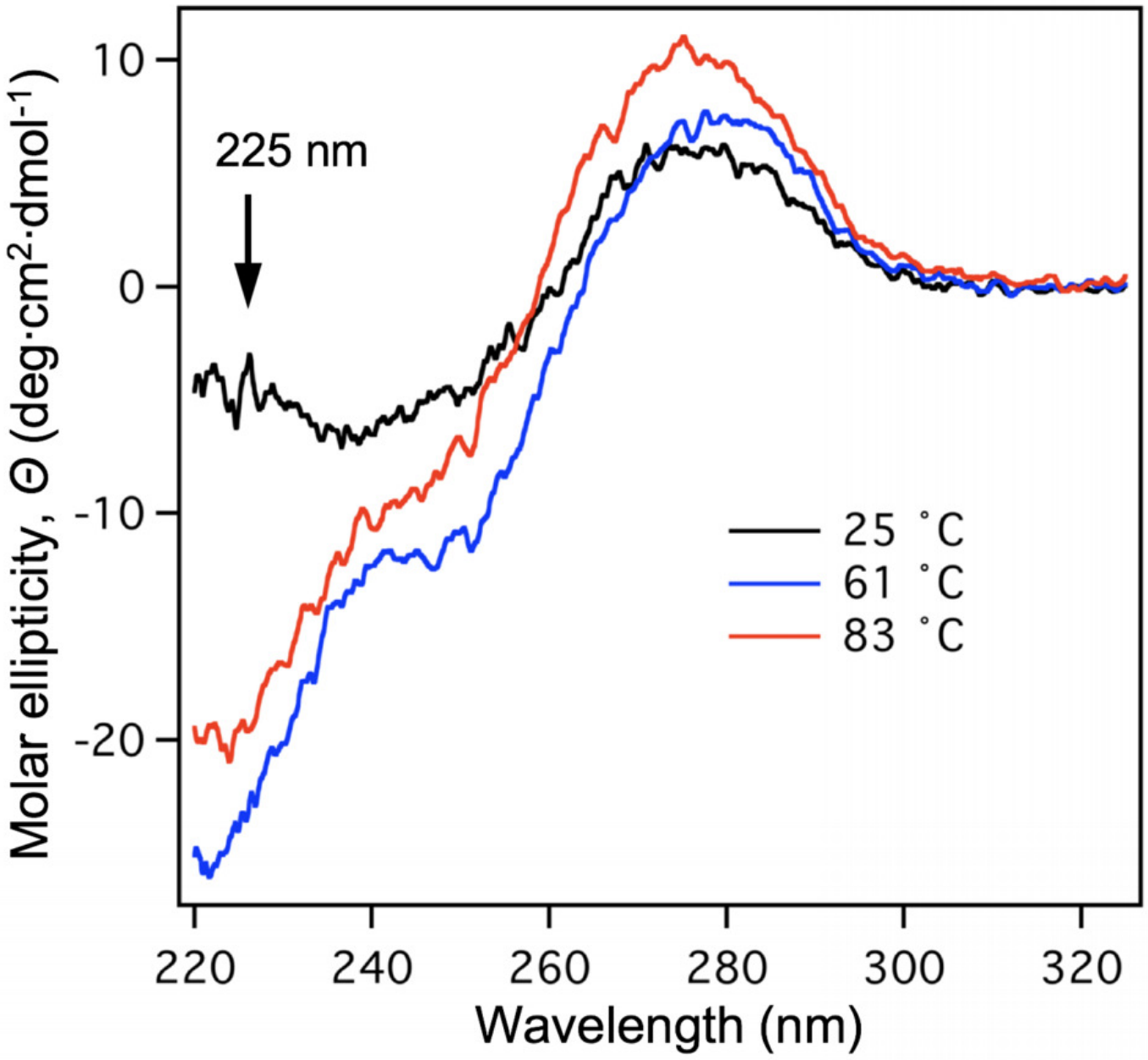

Journal of Virology

JVI

Journal of Virology